Hindawi
Advances in Materials Science and Engineering
Volume 2018, Article ID 2651424, 9 pages
https://doi.org/10.1155/2018/2651424

Research Article

Change of Pore-Fracture Structure of Anthracite Modified by Electrochemical Treatment Using Micro-CT

Xianfa Kong, Junqing Guo, and Tianhe Kang

Institute of Mining Technology, Taiyuan University of Technology, Taiyuan, Shanxi 030024, China

Correspondence should be addressed to Junqing Guo; 13753106501@163.com

Received 4 September 2017; Revised 19 December 2017; Accepted 26 December 2017; Published 21 March 2018

Academic Editor: Yee-wen Yen

The electrochemical method can strengthen gas desorption and seepage from coal. The study on change of the pore-fracture structure of coal after electrochemical modification can help to reveal the mechanism. Anthracite was modified by the electrochemical method using our own self-developed experiment apparatus. The pore-fracture structure of modified samples was measured by micro-CT. Combined with the Matlab software, its characteristics such as pore number, porosity, and average pore diameter were analyzed. The results show that (1) the number of fractures in modified coal samples increases. The shape of new fractures in samples in the anodic and cathodic zones was irregular voids and striola, respectively. The effect of electrochemical treatment on the section of samples close to the electrode is relatively obvious. (2) With increasing pore size, the number of pores in samples changes according to negative exponential rules. After electrochemical modification, the porosity of modified samples in the anodic zone increases from 11.88% to 31.65%, and the porosity of modified samples in the cathodic zone increases from 12.13% to 36.71%. (3) The main reason for the increase in the number of pores of coal samples in the anodic and cathodic zones is the treatment of electrolytic dissolution of minerals and electrophoretic migration of charged particles, respectively.

1. Introduction

The coal-bed methane has attracted widespread attention as clean energy. However, permeability of coal seams is very low—less than 0.001 mD [1, 2], which seriously hampers CBM development or gas extraction.

The methods of improving permeability mainly include protective seam mining [3], hydraulic fracturing [4, 5], hydraulic cutting [6, 7], and blasting-induced fracturing [8]. These approaches have achieved remarkable effect in engineering application; however, the lump coal cut by man-made cracks is still large and some studies indicate that even an inch lump coal requires months or years to release most of its gas and the residual gas content is as high as 38% [9–11]. Therefore, an exploratory study on intensifying methane desorption and seepage from coal modified by electrochemical treatment was proposed [12]. Guo et al. [13] found that the average desorption rate of methane from 130 to 140 mm lump coal after electrochemical treatment increased by 1.68 times reaching desorption equilibrium. In general, the electrochemical method is applicable to soft coal seam [14]. The smaller the lump size of coal is, the more obvious the action effect is. However, the effect of electrochemical treatment on the pore structure of coal has not been quantified.

In the aspect of the pore-fracture structure test of coal, the micro-CT technology is widely used because of nondestructive measurement and direct observation of the inner structure [15–17]. It works by measuring the density distribution of the object using X-ray and presents in the form of gray image by using computer.

Anthracite was modified by the electrochemical method using our own self-developed experiment apparatus. The pore-fracture structure of modified samples was measured by micro-CT scanning. Combined with the Matlab software, its characteristics such as pore number, porosity, and average pore diameter were analyzed, and the change mechanism of coal structure was revealed.

Table 1: The proximate, ultimate, and maceral composition of anthracite.

Coal samples	R^o_{max} (%)	Proximate (%)			Ultimate (%)				Maceral (%)		
		M_{ad}	A_{ad}	V_{ad}	C	H	O	S	V	I	L
The original	2.86	1.65	5.21	6.12	86.52	2.64	6.83	3.32	86.3	13.7	0.0
Modified sample near anode	2.73	0.68	3.15	8.21	85.20	2.72	8.77	2.01	85.7	14.3	0.0
Modified sample near cathode	2.89	0.76	4.08	8.67	85.68	3.14	7.32	2.76	84.1	15.9	0.0

Note: R^o_{max} = vitrinite reflectance; V = vitrinite; I = inertinite; L = liptinite.

Table 2: The test result of coal ash composition.

Coal sample	Coal ash composition (%)								
	SiO_2	Al_2O_3	CaO	Fe_2O_3	SO_3	MgO	TiO_2	Na_2O	P_2O_5
The original	31.86	23.77	19.01	15.93	7.46	0.66	0.94	0.32	0.05
Modified sample near anode	37.83	28.31	12.56	12.32	5.29	0.37	2.31	0.63	0.38
Modified sample near cathode	26.25	18.39	22.93	19.43	8.72	1.83	1.29	0.74	0.42

2. Modification of Coal and Micro-CT Measurement

2.1. Coal Samples. Anthracite was collected from the No. 15 coal seam in the southeast of Qinshui Basin from Sihe coal mine (Shanxi province, China). Two cylindrical specimens with a diameter of 24.83 mm and a length of 25 mm and two cylindrical specimens with a diameter of 2.54 mm and a length of 10 mm were processed using the drilling machine, cutting machine, and polisher machine. The samples were scanned using a micro-CT device and then placed near the anode and cathode in the electrochemical modification apparatus, respectively. The electrolyte was Na_2SO_4 solution with a concentration of 0.05 mol·L^{-1}. The electric potential gradient was 4 V·cm^{-1}. The action time was 120 h. The modified samples were cleaned with distilled water and dried in an oven at 378–383 K until a constant weight was achieved. The samples were scanned at the same test condition using the micro-CT device. In addition, maximum vitrinite reflectance measurements and proximate, ultimate, and maceral composition and coal ash composition analyses were performed following the GB/T 6948-2008, GB/T 212-2008, GB/T 476-2001, GB/T 8899-1998 and GB/T 1574-2007 standard procedures, respectively. The test results are shown in Tables 1 and 2.

It can be seen that the ash content of samples modified in the anodic and cathodic zones decreases from 5.21% to 3.15% and 4.08%, respectively. The major reduction in chemical compositions of the modified samples in the anodic zone is CaO (from 19.01% to 12.56%), Fe_2O_3 (from 15.93% to 12.32%), and SO_3 (from 7.46% to 5.29%). The major reduction in chemical compositions of modified samples in the cathodic zone is SiO_2 (from 31.86% to 26.25%) and Al_2O_3 (from 23.77% to 18.39%).

2.2. Electrochemical Modification Apparatus. The electrochemical modification equipment shown schematically in Figure 1 is composed of a DC power source, a current meter, a wire, an electrolyzer, an electrolyte, electrodes, and coal samples. The output voltage of the DC power source is 0–250 V.

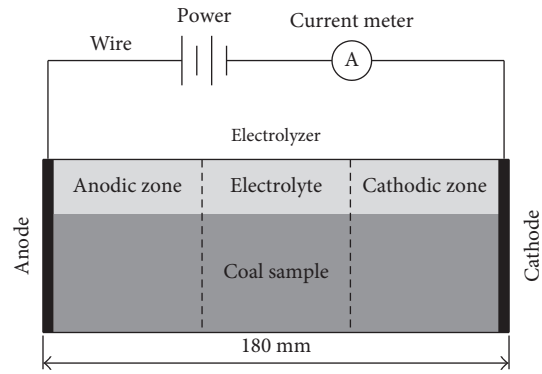

Figure 1: Diagram of the electrochemical modification apparatus.

The electrolyte used in this work is Na_2SO_4 (Sinoreagent, China). Na_2SO_4 is an inorganic salt with strong acid and strong base, which can strengthen the electrical conductivity of solution and guarantee a faster reaction rate. Moreover, the pH of Na_2SO_4 solution is approximately 7, which can ensure the independence of acidity in the anodic zone and alkalinity in the cathodic zone and further, respectively, compare the action effect of these two zones. The electrode is a square graphite sheet with a thickness of 5 mm and a side length of 100 mm.

2.3. Micro-CT Measurement System. The micro-CT system mCT225kVFCB was developed jointly by Taiyuan University of Technology and Chinese Academy of Engineering Physics (Figure 2). The system consists of an X-ray transmitter (Phoenix, Germany), a digital panel receiver (Varian, American), a specimen seat, a seat movement or bit, and so on. The X-ray transmitter launches lasers penetrating and scanning the tested specimen. The scanned images display on the digital panel displayer on the opposite. The maximum magnification of scanned images for the tested specimen can be as large as 400 times. The resolution ratio of scanning element is 0.5 μm–0.194 mm. For the samples with diameters of 24.83 mm and 2.54 mm in this test, the test voltage is

Figure 2: Miro-CT measurement system.

90 kV and 70 kV, respectively. The electric current is 100 μA and 70 μA, respectively. The magnification ratio is 14.39 and 125.67, respectively. The 400 coronal images were filtered and reconstructed using the analysis software of μCT computer system. Then, 1500 slices of each μCT section image were generated in a bit map format (Figure 2).

The scanned CT images are gray images. The gray levels can reflect the density of the scanned material. The brighter a certain part of the image is, the higher the density of material in this zone is. The white, black, and gray areas represent minerals, pores, and coal matrix, respectively. Thus, the pore structure of coal can be obtained. In order to reflect the change characteristics of the pore-fracture structure of coal after modification, the sample was divided into 3 sections on the direction vertical to the bedding plane (Figure 3). The typical cross-section image was selected in each section and conducted comparative analysis.

3. Results and Analysis

3.1. Change of Fracture Structure. Figure 4 shows the fracture structure of the sample with a diameter of 24.83 mm in the anodic zone before and after modification. There are lots of minerals filled in fractures of original samples, which present 3 kinds of distribution type: short lines with a width of 150 μm and a length of 2.5 mm embedded in coal matrix nearly parallel or vertical to filled fractures (Figure 4(a)), long lines with a width of 300–700 μm remaining orthogonal to each other (Figures 4(b) and 4(c)), and round agglomerates with a diameter of 100 μm~3 mm embedded loosely in coal matrix (see the bottom section in Figure 4 (b)).

After electrochemical modification, the inner structure of coal samples in the anodic zone shows three kinds of change: (1)some new fractures and cavities appear, especially around filled mineral, such as zones A1 and A2 in Figure 4(a), zone A1 in Figure 4(b), and zones A1 and A2 in Figure 4(c); (2)existing pores and fractures extend, such as zone B in Figure 4(a), zone B in Figure 4(b), and zones B1 and B2 in Figure 4(c); and (3)coal matrix in the edge of the specimen falls off along the filled mineral zone, such as zone C in Figure 4(a). In a word, the number of fractures in coal in the anodic zone increases and the fracture shape is basically hole.

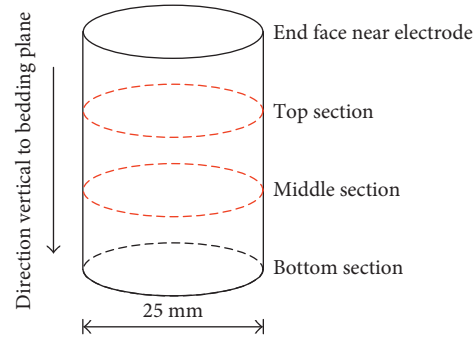

Figure 3: Schematic diagram of trisection along the direction vertical to the bedding plane of coal.

Figure 5 shows the fracture structure of the sample with a diameter of 24.83 mm in the cathodic zone before and after modification. Compared with the original coal sample, the inner structure of coal samples in the cathodic zone shows three kinds of change: (1) filled minerals in the fracture in the top section of the sample disappear, such as zones A1, A2, and A3 in Figure 5(a). Table 3 shows the statistical result of coal matrix size, as can be seen that the space between coal matrix with an average length of 8.5 mm and an average width of 4.68 mm is 300 μm; (2) some minerals disappear, such as zones A1 and A2 in Figure 5(b) and zone A1 in Figure 5(c); and (3) new fractures initiate around filled minerals, such as zones B1 and B2 in Figure 5(c). In a word, filled minerals in the edge of the sample disappear. The number of fractures increases, and the fracture shape is basically thin stripes.

3.2. Change of Pore Structure. The maximum statistical area of the scanned sample with a diameter of 2.54 mm was segmented from the single μCT image using the Matlab software. The statistical area of slice 500 is shown in Figure 6. The initial point was (300, 300) and the side length was 800 pixels in the square statistical areas of Figures 6(a) and 6(b); the initial point was (500, 500) and the side length was 800 pixels in the square statistical areas of Figures 6(c) and 6(d). As can be seen that, after electrochemical modification, the number of minerals filled in the sample in the anodic zone decreases significantly, whereas some minerals in the sample in the cathodic zone aggregate (see zone A in Figure 6(d)).

In order to obtain the change rule of the pore structure of the samples modified in anodic and cathodic, respectively, the porosity is calculated and the numbers of connected groups are counted. The segmented image is being processed by binaryzation, colorInvert, connected group label, and regional colorization, as shown in Figure 7. The same connected group is represented with one color, and the black region represents mineral matter. The porosity of coal samples can be calculated according to (1) and is shown in Table 4:

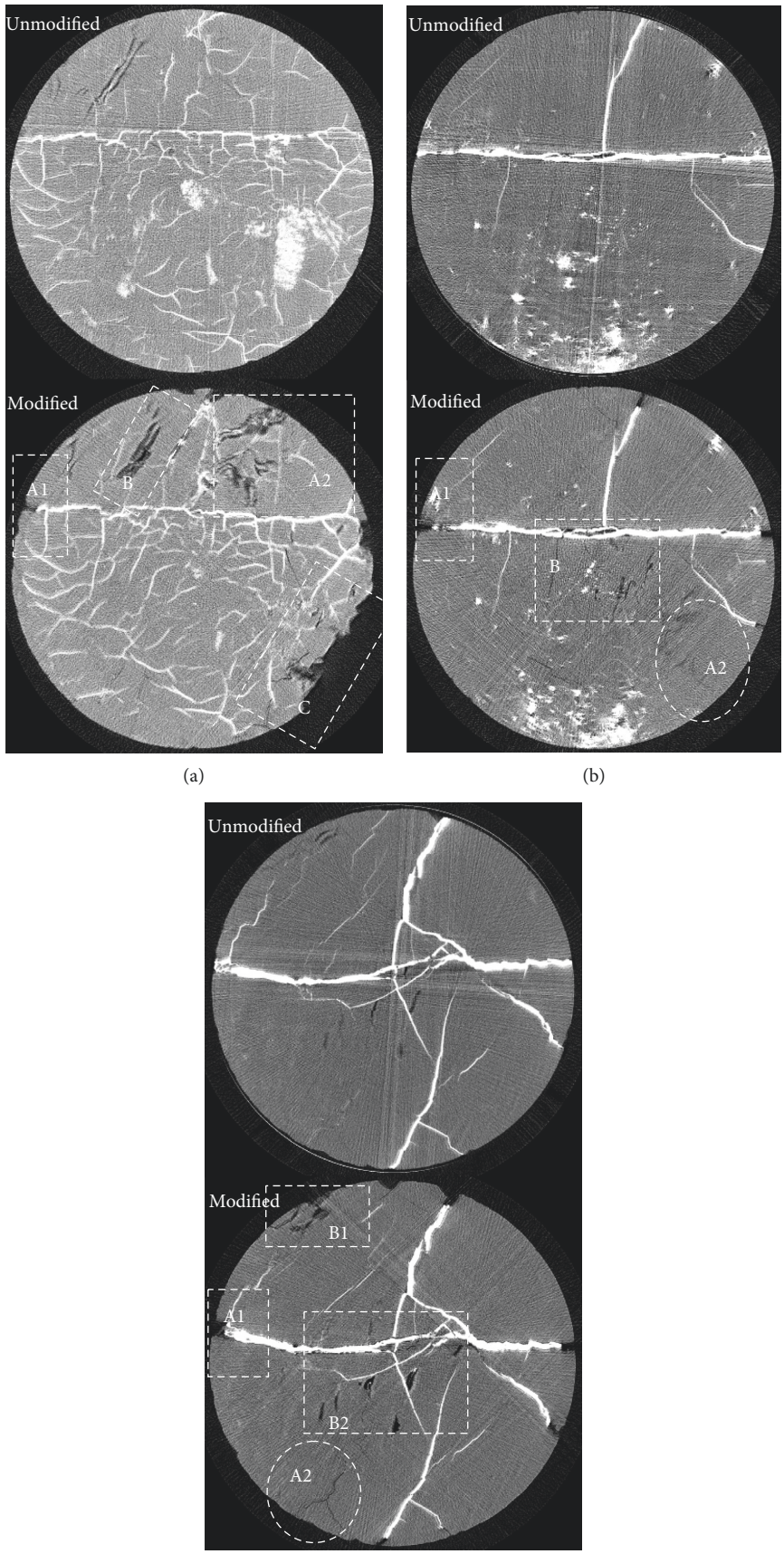

Figure 4: CT image of the structure of coal in the anodic area after modification. (a) Top section, (b) middle section, and (c) bottom section.

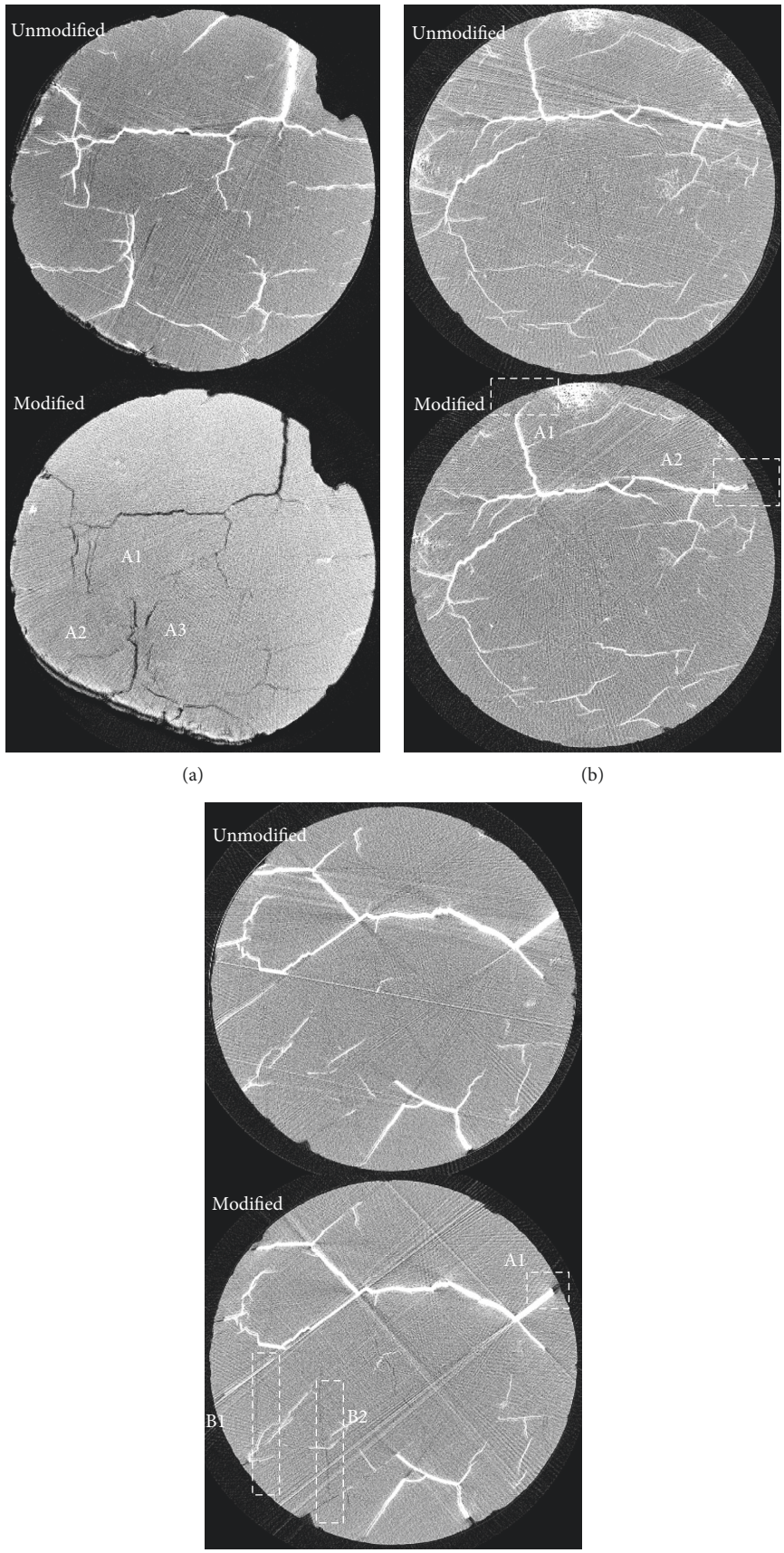

Figure 5: CT image of the structure of coal in the cathodic area after modification. (a) Top section, (b) middle section, and (c) bottom section.

Table 3: The statistical result of the size of coal matrix.

Number	Length (mm)	Width (mm)
A1	10.06	4.07
A2	7.71	5.82
A3	7.74	4.15
Average	8.50	4.68

$$\phi = \frac{N_p}{N_c} \times 100\%, \tag{1}$$

where ϕ is the surface porosity, N_p is the number of pixels of which the gray level is lower than the threshold level, and N_c is the number of all pixels. It can be seen that the porosity of coal matrix after modification increases greatly. The porosity of the coal sample in the anodic zone increases from 11.88% to 31.65%, and the porosity in the cathodic zone increases from 12.13% to 36.71%.

In order to obtain the pore size distribution, the μCT image was analyzed using the Matlab software according to the following steps:

(1) Count the number of pixels in labeled connected groups. Calculate the area of connected groups according to the area of pixels, and then obtain the pore diameter by equivalent conversion.

(2) Count the number of connected groups which have the same counts of pixels, and then obtain the number of pores which have the same pore size and the total pore number, as shown in Table 4. The total pore number of unmodified coal samples in anodic and cathodic zones is 6045 and 6521, respectively. The difference is resulted from the heterogeneity of coal structure and different positions. After modification, the total pore number of samples in anodic and cathodic zones decreases to 3314 and 2896, respectively, illustrating that some pores are connected. Figure 8 shows the pore size distribution of coal samples after modification in anodic and cathodic zones, respectively. With increasing pore size, the number of pores in coal samples changes according to negative exponential rules. The relationship illustrated in Figure 8 can be expressed as follows:

$$\begin{aligned}
&\text{in the anodic zone,}\\
&\text{unmodified:} \quad n = 734\exp(-0.27D) + 1.11, \quad R = 0.9520,\\
&\text{modified:} \quad n = 1069\exp(-0.51D) + 2.83, \quad R = 0.9536,\\
&\text{in the cathodic zone,}\\
&\text{unmodified:} \quad n = 3209\exp(-0.64D) + 8.37, \quad R = 0.9245,\\
&\text{modified:} \quad n = 357\exp(-0.29D) + 0.97, \quad R = 0.9507,
\end{aligned} \tag{2}$$

where n is the number of pores and D is the pore size. After electrochemical modification, the number of micropores decreases and the number of macropores increases significantly. The maximum pore aperture of modified samples in the anodic zone increases from 50.08 μm to 117.94 μm, and the maximum pore aperture of modified samples in the cathodic zone increases from 52.33 μm to 159.77 μm. The amplification is 2.36 and 3.05, respectively.

(3) Calculate the equivalent average diameter of pores according to the total area of pixels and the number of pores, as shown in Table 4. After modification, the average pore size of the sample in the anodic zone increases from 6.09 μm to 20.43 μm, and the average pore size of the sample in the cathodic zone increases from 7.71 μm to 32.77 μm. The amplification is 3.35 and 4.25 times, respectively.

4. Mechanism Analysis

Anthracite is a semiconductor [18] with an electrical conductivity lower than the electrical conductivity of the electrolyte used for this electrochemical modification. The electrical conductivity of anthracite mainly depends on the electrical conductivity of the electrolyte in fractures and pores. In the process of electrochemical treatment, the oxidizing reaction occurs in the anode where H^+ is formed, and the reduction reaction occurs in the cathode where OH^- is formed [14]. The reaction equations are as follows:

$$\text{anode: } 2H_2O - 2e^- \rightarrow O_2 + 4H^+, \tag{3}$$

$$\text{cathode: } 2H_2O + 2e^- \rightarrow H_2 + 2OH^-. \tag{4}$$

In addition, as can be seen in Tables 1 and 2, the ash content of the samples after modification decreases obviously. The decreased ash composition of the samples modified near the anode is mainly CaO, Fe_2O_3, and SO_3. It may be resulted from the electrolytic dissolution of some minerals. The electrolyte in the anodic zone moves osmotically to fractures in coal. The hydrogen ions in the electrolyte can dissolve calcite (Ca) and pyrite (Fe). The filled fractures are connected, as shown in Figure 9. Guo [14] also obtained similar conclusion by SEM. The reaction equations are as follows:

$$CaCO_3 + 2H^+ \rightarrow Ca^{2+} + CO_2 + H_2O, \tag{5}$$

$$FeS_2 + 2H^+ \rightarrow Fe^{2+} + H_2S. \tag{6}$$

The decreased ash composition of the samples modified near the cathode is mainly SiO_2 and Al_2O_3. It may be resulted from electrophoretic migration of clay. The particles (coal powder and clay) which filled generally in pores and coal matrix show negative charge in alkaline solution. Under the action of the electric field, these charged particles move to the anode, which increase the number of pores and

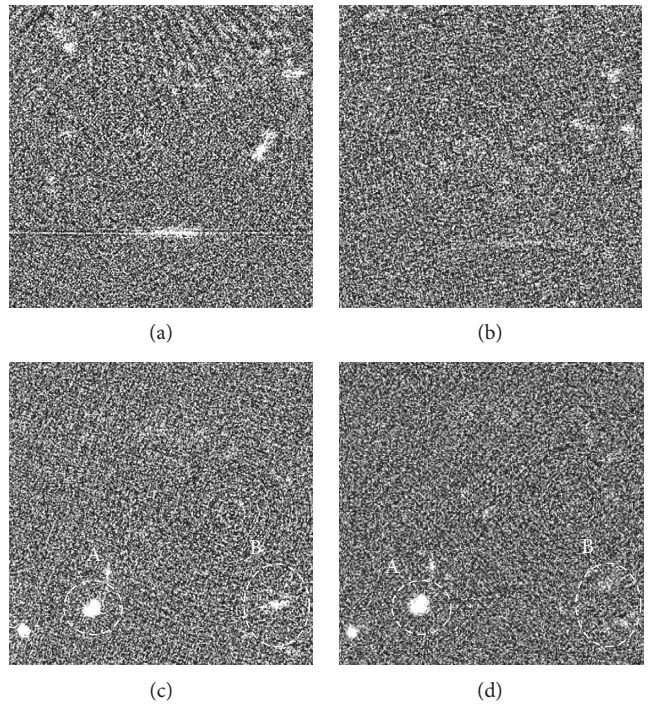

(a) (b) (c) (d)

Figure 6: CT image of the inner structure of anthracite with a diameter of 2.54 mm before and after modification. (a) Unmodified anodic zone, (b) modified anodic zone, (c) unmodified cathodic zone, and (d) modified cathodic zone.

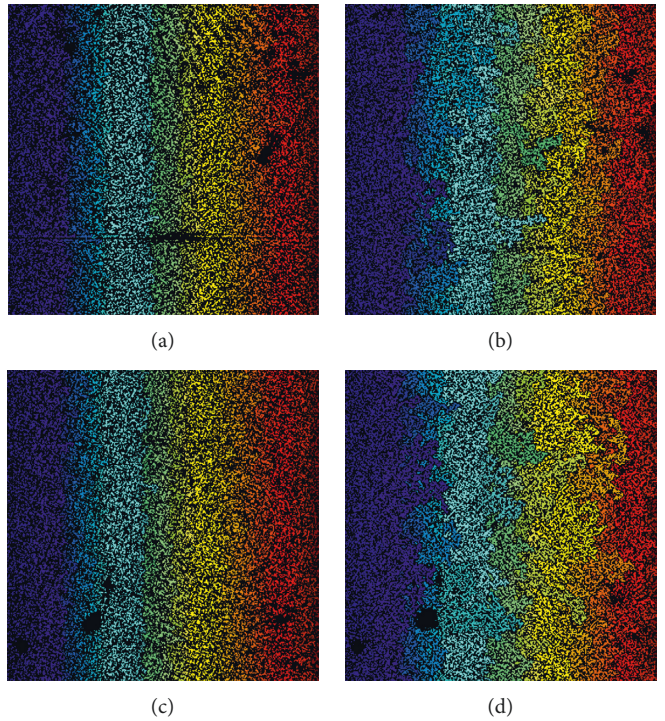

(a) (b) (c) (d)

Figure 7: The distribution of the connected group of anthracite with a diameter of 2.54 mm after modification. (a) Unmodified anodic zone, (b) modified anodic zone, (c) unmodified cathodic zone, and (d) modified cathodic zone.

Table 4: Pore structure parameters of anthracite with a diameter of 2.54 mm.

Name	Porosity (%)	Total pore number	Maximum pore size (μm)	Average pore size (μm)
Unmodified anodic zone	11.88	6045	50.08	6.09
Modified anodic zone	31.65	3314	117.94	20.43
Unmodified cathodic zone	12.13	6521	52.33	7.71
Modified cathodic zone	36.71	2896	159.77	32.77

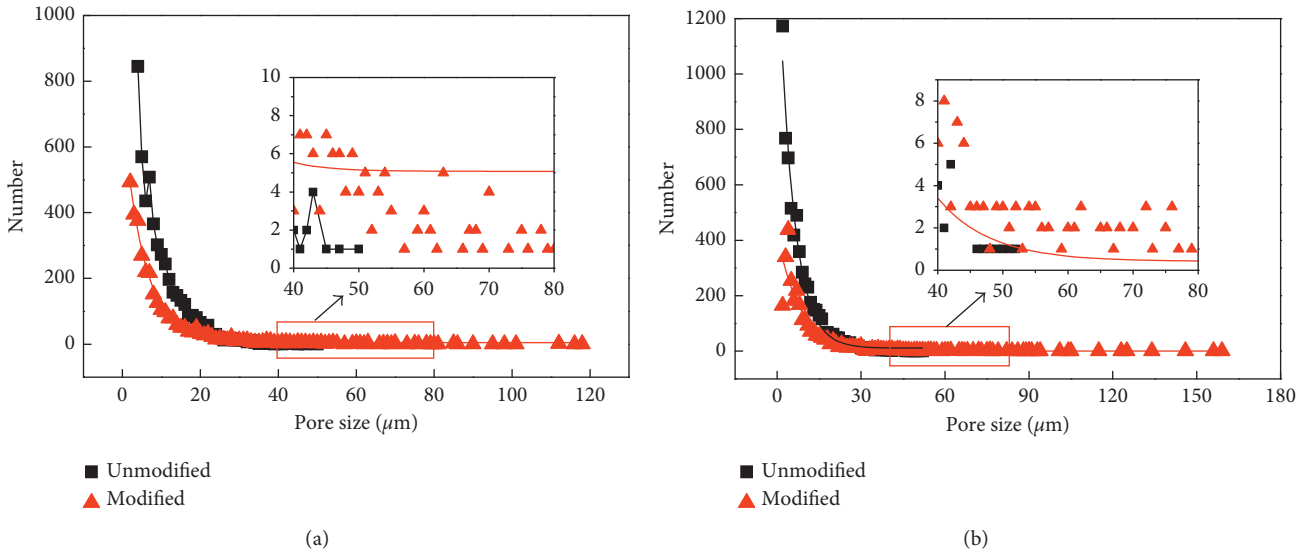

Figure 8: Pore size distribution of samples with a diameter of 2.54 mm before and after modification. (a) Sample modified in the anodic zone; (b) sample modified in the cathodic zone.

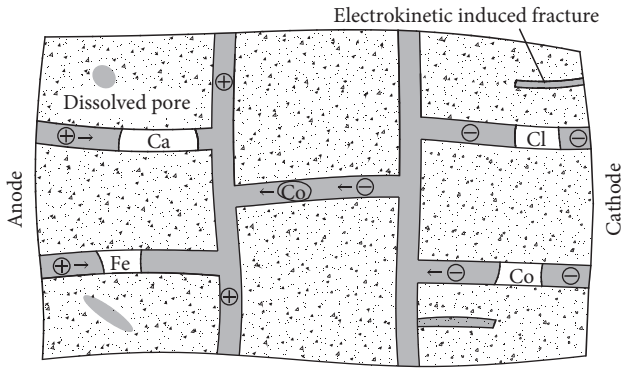

Figure 9: Schematic diagram of the mechanism by which anthracite was modified by the electrochemical method.

provide passage for gas migration. Guo [14] also observed this phenomenon by SEM.

5. Conclusion

(1) The number of fractures in modified coal samples increases. The shape of new fractures in samples in the anodic and cathodic zones was irregular voids and striola, respectively. The effect of electrochemical treatment on the section of samples close to the electrode is relatively obvious.

(2) With increasing pore size, the number of pores in coal samples changes according to negative exponential rules. After electrochemical modification, the porosity and average pore diameter of coal matrix increase. The porosity of modified samples in the anodic zone increases from 11.88% to 31.65%, and the porosity of modified samples in the cathodic zone increases from 12.13% to 36.71%.

(3) The main reason for the increase in the number of pores of coal samples in the anodic and cathodic zones is the treatment of electrolytic dissolution of minerals and electrophoretic migration of charged particles, respectively.

Conflicts of Interest

The authors declare that there are no conflicts of interest.

Acknowledgments

This research was supported financially by the National Natural Science Foundation of China (Grant no. 51174141) and the Basic Research Project of Shanxi Province (Grant no. 201701D221241).

References

[1] Y. Y. Lu, Y. Liu, and X. Li, "A new method of drilling long boreholes in low permeability coal by improving its permeability," *International Journal of Coal Geology*, vol. 84, no. 2, pp. 94–102, 2010.

[2] J. Close, "Natural fractures in coal," in *Hydrocarbons from Coal*, B. E. Law and D. D. Rice, Eds., vol. 38, pp. 119–132, American Association of Petroleum Geologists: AAPG Studies in Geology, Tulsa, OK, USA, 1993.

[3] L. Yuan, "Theory of pressure-relieved gas extraction and technique system of integrated coal production and gas extraction," *Journal of China Coal Society*, vol. 34, no. 1, pp. 1–8, 2009, Chinese.

[4] J. Zhang, "Numerical simulation of hydraulic fracturing coalbed methane reservoir," *Fuel*, vol. 136, pp. 57–61, 2014.

[5] T. Wang, W. Zhou, and J. Chen, "Simulation of hydraulic fracturing using particle flow method and application in a coal mine," *International Journal of Coal Geology*, vol. 121, pp. 1–13, 2014.

[6] Y. Zhao, D. Yang, and Y. Hu, "Study on the effective technology way for mining methane in low permeability coal seamseam," *Journal of China Coal Society*, vol. 26, no. 5, pp. 455–458, 2001, Chinese.

[7] F. Yan, B. Lin, and C. Zhu, "A novel ECBM extraction technology based on the integration of hydraulic slotting and hydraulic fracturing," *Journal of Natural Gas Science and Engineering*, vol. 22, pp. 571–579, 2015.

[8] H. Kumar, E. Lester, and S. Kingman, "Inducing fractures and increasing cleat apertures in a bituminous coal under isotropic stress via application of microwave energy," *International Journal of Coal Geology*, vol. 88, no. 1, pp. 75–82, 2011.

[9] W. R. Bodden and R. Ehrlich, "Permeability of coal and characteristics of desorption tests: implications for coalbed methane production," *International Journal of Coal Geology*, vol. 35, no. 1–4, pp. 333–347, 1998.

[10] D. Masszi, *Cavity Stress-Relief Method for Recovering Methane from Coal Seams*, pp. 149–154, Rocky Mountain Association of Geologists, Denver, CO, USA, 1991.

[11] G. E. Eddy, C. T. Rightmire, and C. W. Bryer, "Relationship between methane content of coal rank and depth: theoretical vs. observed," in *Proceedings of SPE Unconventional Gas Recovery Symposium*, vol. 345–10, Pittsburgh, PA, USA, May 1982.

[12] T. H. Kang, "A method of intensifying gas desorption and seepage from coal by electrochemical method," ZL201110130935.8, 2013, Chinese.

[13] J. Guo, T. Kang, and J. Kang, "Accelerating methane desorption in lump anthracite modified by electrochemical treatment," *International Journal of Coal Geology*, vol. 131, pp. 392–399, 2014.

[14] J. Guo, *Research on Characteristics and its Mechanism of Intensifying Gas Desorption and Seepage of Anthracite by Electrochemical Method*, Taiyuan University of Technology, Taiyuan, China, 2015, Chinese.

[15] C. O. Karacan and E. Okandan, "Fracture/cleat analysis of coals from Zonguldak Basin (northwestern Turkey) relative to the potential of coalbed methane production," *International Journal of Coal Geology*, vol. 44, no. 2, pp. 109–125, 2000.

[16] W. Soto-Acosta, A. Schimmelmann, and M. Mastalerz, "Diagenetic mineralization in Pennsylvanian coals from Indina, USA: $^{13}C/^{12}C$ and $^{18}O/^{16}O$ implications for cleat origin and coalbed methane generation," *International Journal of Coal Geology*, vol. 47, pp. 51–62, 2001.

[17] S. Mazumder, K.-H. A. A. Wolf, K. Elewaut, and R. Ephraim, "Application of X-ray computed tomography for analyzing cleat spacing and cleat aperture in coal samples," *International Journal of Coal Geology*, vol. 68, no. 3-4, pp. 205–222, 2006.

[18] J. Podder and S. Majumder, "A study on thermal and electrical characterization of Barapukuria coal of northwestern Bangladesh," *Thermochimica Acta*, vol. 372, no. 1-2, pp. 113–118, 2001.